PROJEKT ZÁRÓ BESZÁMOLÓ

„Design and Development of Highly Active and Stable Nano-Structured Catalyst for Dry Reforming of Methane with CO_2" című NN75009 számú (Erachemistry) OTKA által támogatott kutatásról

1.1. Introduction and short scientific background

Among the different routes to produce synthesis gas from coal, oil or natural gas dry reforming is the reaction leading to the lowest H_2/CO ratio (1:1), which is a desired feedstock in the chemical industry for the synthesis of oxygenates. Methane dry reforming (DRM) with carbon dioxide is of a great interest for environmental protection as well, since the reaction consumes two important greenhouse gases (CH_4 and CO_2). Moreover, there are several natural gas wells in Hungary, which contain large amounts of CO_2 (> 30 %) beside methane, and these wells are now closed due to the low BTU value of the gas. It seems that DRF reaction indeed deserves the ever increasing attention in the field of catalytic research.

Dry reforming of methane (1) can be described by the following reaction:

$$\mathbf{CH_4 + CO_2 \Leftrightarrow 2CO + 2H_2} \quad (1) \qquad (\Delta H_{1100K} = +260 \text{ kJ mol}^{-1})$$

which is strongly endothermic and based on the equilibrium constant the transformation is feasible only above 915K ($\Delta G=0$) at atmospheric pressure, therefore, high temperatures (~800-900 °C) are required to reach significant conversion levels. There are side reactions which can reduce the efficiency of the dry reforming of methane through inactive coke formation:

$CH_4 \Leftrightarrow C + 2H_2$ (2) (methane decomp., ΔH_{1100K}= 90.7 kJ mol^{-1}, $\Delta G=0$ at 810K)

$2CO \Leftrightarrow C + CO_2$ (3) (Boudouard reaction, ΔH_{1100K}= -170 kJ mol^{-1}, $\Delta G=0$ at 975K)

Depending of the reaction temperature, reaction (3) could favour coke deposition or coke removal. It is important to note that the reverse water-gas shift reaction also occurs thus reduces the H_2/CO ratio[1]:

$CO_2 + H_2 \Leftrightarrow CO + H_2O$ (4) (RWGS, ΔH_{1100K}= 38 kJ mol^{-1})

Or the water formed in reaction (4) reacts with surface carbon:

$H_2O + C \Leftrightarrow CO + H_2$ (5) (ΔH_{1100K}= 135 kJ mol^{-1}).

It is seen, that under the conditions of dry reforming, carbon formation on the surface of catalyst is also thermodynamically favored, and carbon deposits will be formed if the rate of methane dissociation is faster than the oxidation of carbon, which can occur with oxygen formed by CO_2 dissociation on the metal component or with oxygen from carbonates formed at the metal support interface. Coke formation can be severe and even lead to a complete blockage of the reactor under industrially relevant reaction conditions.

The reaction is catalyzed by all VIII transition metals except osmium. In particular, Ni has been studied extensively, being the most active, cheap and available metal. Its main drawback is represented by carbon formation, metal sintering and metal oxidation.

1.2. Outline of the research work reported

In the Institute of Isotopes, the problem of carbon deposition on catalysts has been tackled using bimetallic nanoparticles, while in the University of Limerick, improvements in high-temperature Ni-based steam reforming catalysts have been achieved by modification with various oxides (La_2O_3, Nb_2O_5, etc.). At Strasbourg the approach for dry reforming was to prepare and test some defined oxide structures like perovskites (ABO_3), spinels (A_2BO_4), fluorite ($A_2B_2O_8$), olivine $(Mg_{1-x}Fe_x)_2SiO_4$ as precursors of the catalysts. This background knowledge was put together in this common work.

The present project was aimed to develop new nickel catalysts characterized by nanosized particles stable at high temperature and for longer time and tolerant to the presence of

deposited carbon. The adopted strategies involved to act on the two important catalyst components: a) the support with high surface area and of different nature and b) the active site by promoting it adding other metals such as Au, Rh and Co, possibly inhibiting the carbon formation and also acting as Ni particle size stabilizer.

In the next sections the results are divided into two main groups based on the different supports applied ($MgAl_2O_4$ or Ce-Zr-oxides). Large part of the work is already published, but there are a lot of interesting results that will be put together in the form of one or two papers in the very near future. First, the main experimental techniques and processes will be briefly introduced.

2. General preparation methods, main experimental techniques applied

Here only the common methods are mentioned which were applied during our research focused on the Ce-Zr-oxide- and $MgAl_2O_4$-supported Ni dry reforming catalysts. There were a few special techniques or modification of the basic processes not common for the 2 main topics of the work. These are introduced shortly in the actual section.

For the preparation of catalysts, impregnation, pseudo sol-gel and aqueous sol method was applied. Ce-Zr-oxides synthesized by sol-gel method and commercial $MgAl_2O_4$ spinel were applied as supports.

The phase composition of crystalline components of selected samples was investigated by X-ray diffraction (XRD). The crystallite size for each phase was determined from the full width at half maximum of the first peak using the Scherrer-equation.

Determination of metal content of the samples was done either by radioisotope induced X-ray fluorescence spectrometry (XRF) method or Prompt Gamma Activation Analysis (PGAA).

The distribution and the size of metal particles were studied by a conventional transmission electron microscope (TEM) equipped with energy dispersive spectrometer (EDS) for electron probe microanalysis. High resolution transmission electron microscope (HRTEM) investigations were carried out in some cases as well.

The reducibility of selected catalysts was studied by temperature programmed reduction (TPR) using ~ 0.05 g sample heated from room temperature to 800-900°C under 10%H_2/He flow.

The oxidation state and surface concentration of Ni were determined by XPS performed by a KRATOS XSAM 800 XPS machine equipped with an atmospheric reaction chamber. Spectra were taken in "as prepared" form of the samples and after different in situ or ex situ treatments. AlK_α excitation and 40eV Pass Energy was used during data acquisition. The binding energies (BE) were determined relative to C1s at 285 eV.

The amount of carbon on the sample surface after catalytic run with CH_4/CO_2 = 70/30 feed was estimated from the amount of CO_2 evolved in TPO experiments carried out in 10 vol. % O_2 and 1 vol.% Ar in He. Mass spectrometer was employed to detect CO_2 formation. Using the correlation between the intensity and flow ratio of CO_2 to Ar, the flow of CO_2 could be determined and then integrated through the time, which resulted in the amount of CO_2 formed. Weight of carbon was calculated on the bases of amount of CO_2.

A usual catalytic reaction was performed using CH_4/CO_2 = 70/30 mixture without any diluting inert gas. 0.1-0.03 g of catalyst was put into the quartz reactor and the reactant mixture with 20 ml/min flow rate (total space velocity 12L/gh) was introduced after a reduction pretreatment at 750°C. Temperature during the reaction was raised up to about 800°C until all the CO_2 was consumed (standard reaction with temperature ramp). When repeated reactions were carried out, the reduction treatment at 750°C took only 30-60 min after TPO at 750°C/30 min (that served as calcination). A quadrupole mass spectrometer (type Balzers 100) was used for analysis of the reaction products and the methane and carbon dioxide conversions were calculated[2]. At the beginning of work the calculation of the conversion was based on the assumption that only methane dry reforming takes place (and no other side reactions). It has to

be mentioned that in methane dry reforming reaction there is an obvious dilatation of the gas mixture upon the reaction. At any α conversion of methane the sum of flow rates always higher than the sum of initial flow rates of methane and CO_2 ($F\text{in}^{CH_4}+F\text{in}^{CO_2}$). Therefore, the methane concentrations, before and after the reaction, cannot be used directly for determination of methane conversion. In our practice this problem has been overcome by using the ratio of flow rates (CO to methane) instead of methane concentration. Later on, calibration with H_2 allowed us to estimate the real CH_4 conversion and determine the CO/H_2 ratios (only in the last part of the work).

Long term (overnight) stability tests for 20-24 hours were carried out in two different ways. On the one hand, a standard reaction with temperature ramp up to 750-800^{o}C was conducted on fresh, calcined and reduced sample, then the system was cooled down to 650^{o}C in CO_2+CH_4 mixture and the stability measurement was started at that point and lasted for about 24 hours. On the other hand, the as prepared and pretreated (calc/red) catalyst was ramped in the reaction mixture up to 650^{o}C and left there for the stability measurement. In this case zero in the time scale means the point when 650^{o}C was reached. During the stability tests the main stream of the effluent gas mixture was connected to a gas chromatograph Chrompack 900 and CO, CO_2 and CH_4 were separated on a 5 m long 60/ 80 Carboxen 1000 column, or the gas mixture was measured directly by QMS.

3. Investigations on Ce-Zr-oxide supported catalysts

According to the widely accepted mechanism of dry reforming, CH_4 is adsorbed on metal in a dissociated form to produce hydrogen and hydrocarbon or carbon species ($CH_{x=0-3}$). Both CH_x and H atoms are attached to the metal active sites and then H atoms are recombined and desorbed into the gas phase. The nature of the support can greatly influence the fate of reaction intermediates and the extent of coking. Over a basic support CO_2 activation is suggested to happen on the support in close vicinity of metal particle via formation of carbonates. The carbonate is then reduced by CH_x species to form CO[3]. On acidic support CO_2 chemisorption and dissociation happen on metal, and as the reaction proceeds, highly dehydrogenated carbon deposits accumulate which eventually undergo aging and graphitization and block the metal sites for CO_2 activation, thus loss of activity happens by coke deposition. There are two approaches to avoid or decrease the substantial carbon formation: the first is to choose appropriate support and the second one is to modify the most frequently used nickel metal with a second one.

Ceria and zirconia seem to be promising supports for methane dry reforming. Ceria addition results in usually higher dispersion of active phase and excellent resistance against carbon deposition[4, 5]. The main effect of ZrO_2 is quite similar to that of CeO_2: it causes higher stability due to the strong inhibition of the carbon formation[6], because on ZrO_2 oxygen intermediates are dissociated and better react with carbon species[7]. The simultaneous presence of Zr and Ce-oxides is also beneficial. Rezaei and co-workers synthesized high surface area mesoporous nanocrystalline zirconia with pure tetragonal crystalline phase and doped with 3 % Ce phase to produce excellent support for nickel catalysts in methane dry reforming[8, 9, 10].

One has to note that methane dry reforming test reactions are usually carried out with diluted reactants and so they are far from the realistic conditions. There are a few examples in the literature reporting methane dry reforming on Ce-Zr oxides without any diluting gas[11]. Daza et al. investigated Ce-promoted Ni/Mg-Al samples derived from hydrotalcites[12]. They concluded that Ce promotes the reduction of Ni, acidic support favours the growth of carbonaceous deposits and basic character facilitates carbon gasification. Under “drastic conditions” filamentous coke formation was demonstrated on the catalysts[13].

With excess amount of methane (CH_4/CO_2=2) Montoya et al. studied Ni/ZrO_2-CeO_2 sol-gel catalysts for dry reforming of methane, and declared that phase transformation, support sintering and not coke formation was the main cause of the deactivation. Solid solution of

CeO_2-ZrO_2 was formed by adding 1, 8, 20% CeO_2 to 15%Ni/ZrO_2. It was stated that Ce-oxide prevented the tetragonal to monoclinic transformation of ZrO_2 and the part of Ni^{2+} was incorporated in ZrO_2, but CeO_2 was partially segregated in the case of 20% CeO_2[14].

Our aim was to study the Ce-Zr oxide based metal catalysts prepared by sol-gel technique or impregnation method to gather information about their structure, activity and the different carbonaceous species formed during CH_4 dry reforming with CO_2.

3.1. Structure and catalytic behaviour of Ce-Zr-oxide supported Ni, NiRh and NiCo catalysts prepared by sol-gel technique

The monometallic Ni and bimetallic NiRh and NiCo catalysts were prepared by pseudo sol-gel method based on thermal decomposition of metallic propionates[15,16]. The metal and the oxide precursors (mainly acetates) were dissolved in the excess of propionic acid and the solutions were heated under reflux until evaporation of the solvent. The resulting gel was then calcined in air at 750°C for 4 hours. Monometallic Ni samples were prepared with two different Ce/Zr ratio (see Table 1). The reference Ni/Ce_2Zr_2 (imp) catalyst was prepared by wet impregnation of $Ce_2Zr_2O_8$ sol-gel support with nickel (II) nitrate.

Table 1. The major parameters of the samples

Catalysts	Abbreviation	Ni nominal wt.(%)	Me nominal wt.(%)	BET surf. area (m^2/g)	Lattice parameter (Å)	Support particle size (nm)
5%Ni/$Ce_2Zr_2O_8$	Ni/Ce_2Zr_2 (imp)	5	–	17	5.27	6
$Ce_{0.6}Zr_{2.97}Ni_{0.43}O_{8-\delta}$	$NiCe_{0.6}$ $Zr_{2.97}$ (sg)	5	–	15	5.17	7
$Ce_2Zr_{1.51}Ni_{0.49}Co_{0.29}O_{8-\delta}$	$NiCoCe_2Zr_{1.51}$ (sg)	3	2	11	5.30	7
$Ce_2Zr_{1.51}Ni_{0.49}Rh_{0.03}O_{8-\delta}$	$NiRhCe_2Zr_{1.51}$ (sg)	4.5	0.5	21	5.30	6
$Ce_2Zr_{1.5}Ni_{0.5}O_{8-\delta}$	$NiCe_2Zr_{1.51}$ (sg)	5	–	18	5.29	7

The XRD patterns of the samples after calcination matched well to the face-centered cubic structure of $Ce_{0.6}Zr_{0.4}O_2$ (JCPDS 38-1439). Nevertheless, a purely crystalline NiO, with (001) and (200) planes could also be observed for all samples except $NiCe_{0.6}Zr_{2.97}$ (sg). We suggest that this difference for NiCeZr (sg) catalysts is due to to the varying Ce/Zr ratio. It might be explained by partial rejection of Ni from the host Ce-Zr structure. It was demonstrated that 5 wt% metal cannot be inserted into host Ce-Zr fluorite structure[17]. For the bimetallic catalysts no evidence of Co or Rh oxides was observed. For $NiCoCe_2Zr_{1.51}$ (sg) catalyst it is nickel, which should be rejected due to the difference in ionic radii of Co^{2+} (75pm), Ni^{2+} (69pm) and Zr^{4+} (84pm) after calcination.

Figure 1 shows TPR data on $NiCe_{0.6}Zr_{2.97}$ (sg), $NiCe_2Zr_{1.51}$ (sg) and Ni/Ce_2Zr_2 (imp) samples. The impregnated Ni sample (Fig. 1b) is reduced at lower temperature. The hydrogen consumption at ca. 310-320°C is assigned to the reduction of NiO particles free of interaction and the peak at 380-420°C could correspond to nickel-oxide incorporated into the Ce-Zr structure (meaning that small part of nickel could be integrated into the fluorite framework by impregnation). For Ce-Zr oxide, two small peaks at 600°C and 780°C have been evidenced[18]. In Fig 1 a, peak at 600°C could be also attributed to ceria reduction helped by the presence of reduced nickel. For Ni/Ce_2Zr_2 (imp) reduction of ceria occurs more slowly between 550°C and 730°C. Furthermore, the less the reduction temperature, the bigger the size of Ni particles will be (TEM).

According to transmission electron microscopy (TEM) measurements, in the as prepared state of the sol-gel samples after initial calcination nickel and the other metals are intimately

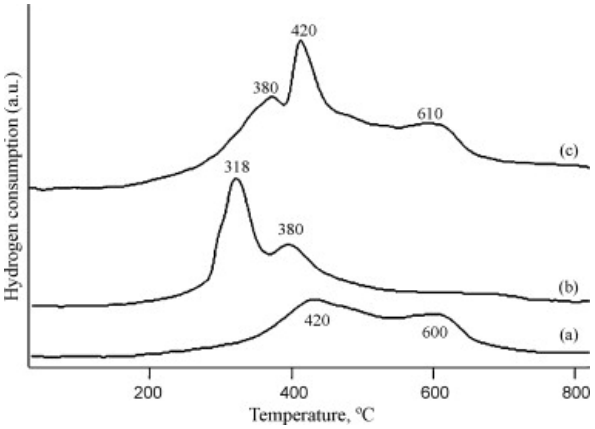

incorporated in a solid Ce-Zr-oxide composite material which is rather compact, and sign of larger metal-oxide particles is hardly seen. In the case of the impregnated sample 2 types of Ni-oxide species were detected: fine Ni-oxide that is incorporated in the oxide matrix and agglomerated 50-150 nm large Ni-oxide particles detached from the support surface. As for the bimetallic samples, Co is seen by EDS analysis, while the amount of Rh seen by EDS technique was only slightly above the detection limit.

Fig. 1. TPR profiles of (a) $NiCe_{0.6}Zr_{2.97}$ (sg); (b) Ni/Ce_2Zr_2 (imp); and (c) $NiCe_2Zr_{1.51}$ (sg) catalysts.

Catalytic activity of the samples in a standard reaction with temperature ramp is shown in Figure 2. The most active sample was $NiRhCe_2Zr_{1.51}$ (sg) catalyst, the second one was $NiCe_{0.6}Zr_{2.97}$ (sg), while $NiCe_2Zr_{1.51}$ (sg) sample proved to be the worst catalyst, although the difference between the conversions vs. temperature curves is small. In a second reaction a decreased activity was observed for all the samples (not shown here), however, after regeneration (TPO+reduction) the original activity could be regained. It was interesting to note that on $NiRhCe_2Zr_{1.51}$ (sg) sample, if TPO was not followed by reduction, the CO_2 conversion curve was the same as after normal regeneration (TPO+reduction step), meaning that the Rh containing sample is able to get reduced by the gas at low temperature. The stability of catalysts at 650°C during overnight reaction was also measured as shown in Figure 3. Note that these tests were carried out on catalyst samples previously used in a standard reaction with temperature ramp, that means carbonaceous contamination formed up to 750-800°C were already present on their surface. Co and Rh containing samples seem to be stable catalysts, the impregnated Ni catalyst only slightly, while sol-gel monometallic Ni samples slowly but surely deactivate during 24 hours. The addition of 0.5 wt% Rh apparently prevents the long term deactivation during overnight test. However, $NiRhCe_2Zr_{1.51}$ (sg) sample shows the largest activity decrease after a standard reaction with temperature ramp, since the CO_2 conversion in Figure 3 is only 48% compared to the conversion value of the fresh, calcined and reduced sample (corresponding data point at 650°C in Figure 2). Thus, we can declare that the Rh-containing sol-gel sample besides the high activity has a high tendency for fast, initial deactivation but then stable activity is maintained for even 24 hours. Addition of Co turns to be more favourable, since the presence of Co also improves catalyst stability but provides higher CO_2 and CH_4 conversion after 24 hours than the Ni,Rh sol-gel sample. However, we should keep in mind that Co content is 2 wt% compared to the 0.5 wt% Rh content of $NiRhCe_2Zr_{1.51}$ (sg). Studies on Ni and Co-containing perovskite-type oxide catalysts revealed the synergetic effect of Ni and Co contributing to catalyst stability[19, 20], while other work showed that cobalt decreased the methane reforming activity of Ni[21]. We can conclude that our catalytic test reactions proved the beneficial effect of 0.5wt% Rh and 2 wt% Co on catalyst stability, while, as for the sol-gel Ni samples, the higher Zr content in the mixed oxide support resulted in a more active but still deactivating catalyst. It is interesting to note the relatively good catalytic performance of the impregnated Ni catalyst.

One possible reason of decreasing activity of the catalyst is the coke formation that gradually blocks catalyst active sites for methane dry reforming reaction. In order to study the surface carbonaceous deposits formed during the reaction, temperature programmed oxidation (TPO) of the surface carbon was performed.

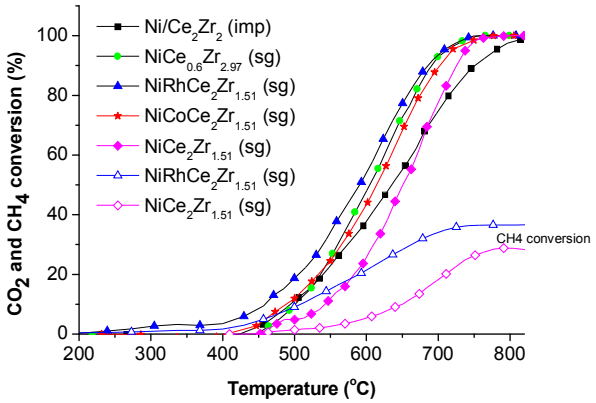

Fig. 2. Comparison of CO_2 conversion curves (and CH_4 conversion of the most and least active samples) in the first reaction after reduction treatment at 750 °C/4 h. Reaction conditions: total space velocity: 12 L h^{-1} g^{-1}; temperature ramp 10 °C/min.

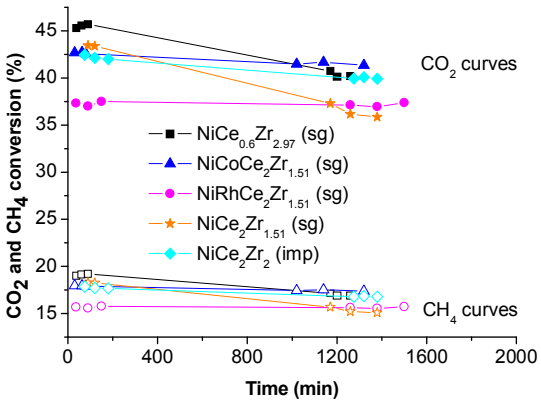

Fig. 3. Long term stability tests at 650 °C on "spent" samples.

The T_{max} obtained in TPO curves may be characteristic of the carbon bond strength to the catalyst surface, reflects the kinetics of carbon burning process, while the CO_2 amount evolved during the oxidation enables quantitative comparison. The results obtained are summarized in Figure 4 (a)-(e). $NiCe_{0.6}Zr_{2.97}$ (sg), $NiCe_2Zr_{1.51}$ (sg) and $NiCoCe_2Zr_{1.51}$ (sg)) samples were the least contaminated (1-3 mg C/100 mg catalyst depending on the conditions prior to TPO), $NiRhCe_2Zr_{1.51}$ (sg) had a medium amount of surface carbon of 4-10 mg while the highest amount of carbon was retained by the surface of 5 % Ni impregnated on Ce_2Zr_2-oxide support (7-12 mg C). The results reflect that there is no straightforward relation between catalytic activity and the amount of surface carbon measured.

The Ni samples produced CO_2 in a single peak but with 200°C of difference depending on the preparation method: sol-gel samples had a peak maximum at 400°C, while the position of TPO peak maxima was shifted to 600°C for the impregnated catalyst (however, note the small shoulder at 400°C). In the case of bimetallic sol-gel samples the low and the high temperature peak was simultaneously observed but each one shifted to lower values, to 350°C and about 500°C. Furthermore, the ratio between low and high temperature peaks apparently changed which points to the alteration of catalyst/carbon structure after repeated reactions and changes with the nature of the second metal. In the case of $NiRhCe_2Zr_{1.51}$ (sg) catalyst less high temperature carbon was observed.

Close investigation of TPO data reveals that the amount of carbon recovered slightly decreases on spent samples (see 1st, 2nd and 3rd TPO data). We observed also that the amount of carbon after the overnight reaction is sometimes lower than in a single reaction with temperature ramp in agreement with Verykios et al. who detected decreased amount of carbon on Rh/Al_2O_3 after 2 h of reaction[22, 23] or the findings of Goula et al. who observed that the amount of carbon increased or decreased after 15 min time on stream depending on the catalyst[24]. Chen et al. also detected that cyclic carbon formation – gasification reduced the filamentous carbon formation[25].

After high temperature oxidation/reduction treatments and catalytic reactions, TEM provides us information about the structural changes happened and the type of carbonaceous deposits formed. TEM images of $NiCe_{0.6}Zr_{2.97}$ (sg) in Figure 5 a and b shows that certain amount of Ni is in strong interaction with the support probably still included in the oxide matrix, while there are Ni particles of 5-80 nm inside carbon nanotubes and encapsulated by graphitic layers separated from the parent mixed oxide support. Figure 5 c clearly indicates that catalyst with higher Ce/Zr ratio did not produce filamentous carbon during overnight run, and the electron diffraction (SAED pattern, not shown here) in this case detected Ni in oxidic form.

The small size[26] and the (partially) oxidized state of nickel probably caused by higher amount of Ce in the support might be the reasons for the lack of nanotubes in $NiCe_2Zr_{1.51}$.

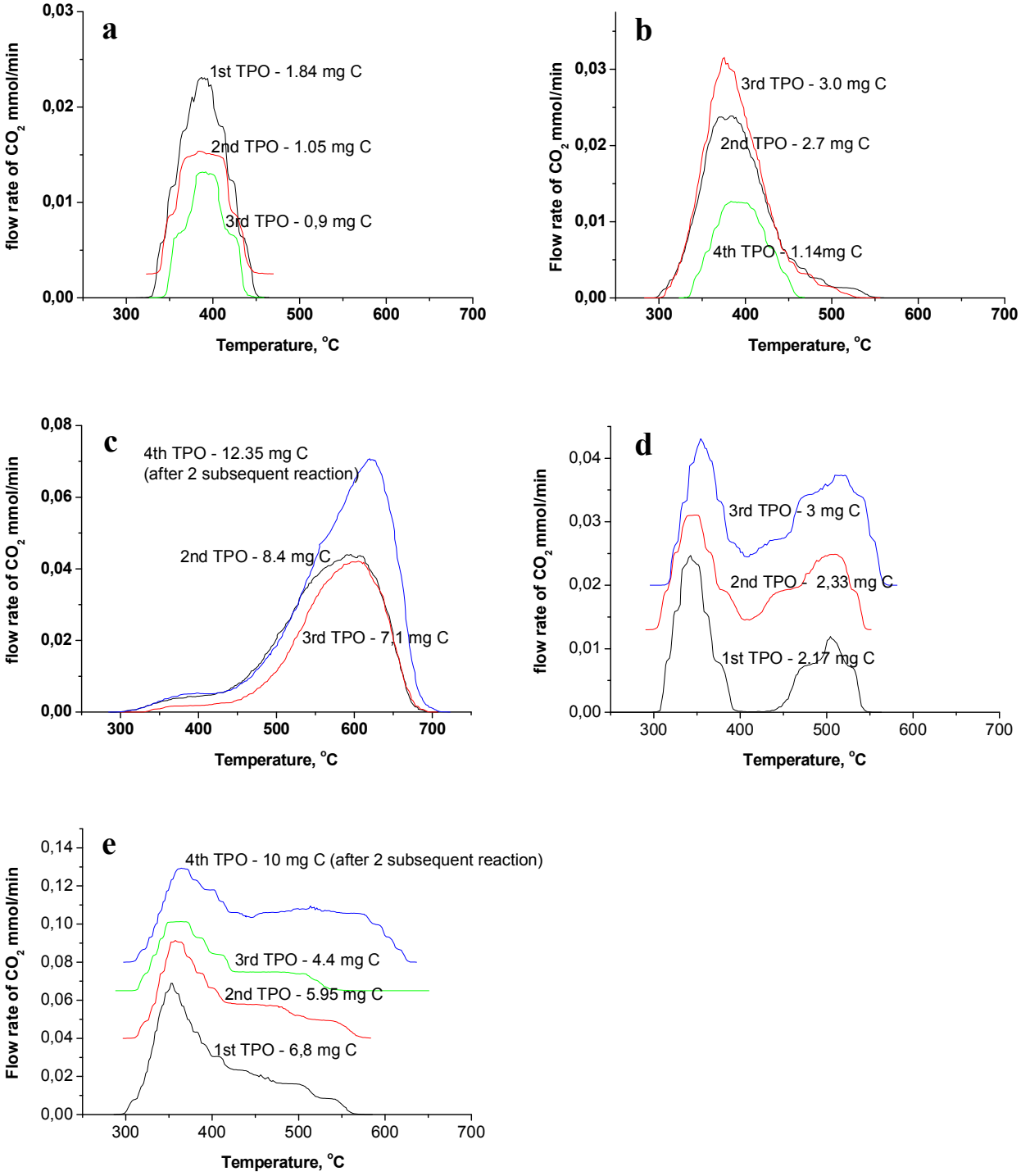

Fig. 4. TPO measurements on: (a) $NiCe_{0.6}Zr_{2.97}$ (sg); (b) $NiCe_2Zr_{1.51}$ (sg); (c) Ni/Ce2Zr2 (imp); (d) $NiCoCe_2Zr_{1.51}$ (sg) and (e) $NiRhCe_2Zr_{1.51}$ (sg). Before each TPO a catalytic reaction with temperature ramp was conducted on the regenerated sample. In some cases curves are shifted for the sake of clarity.

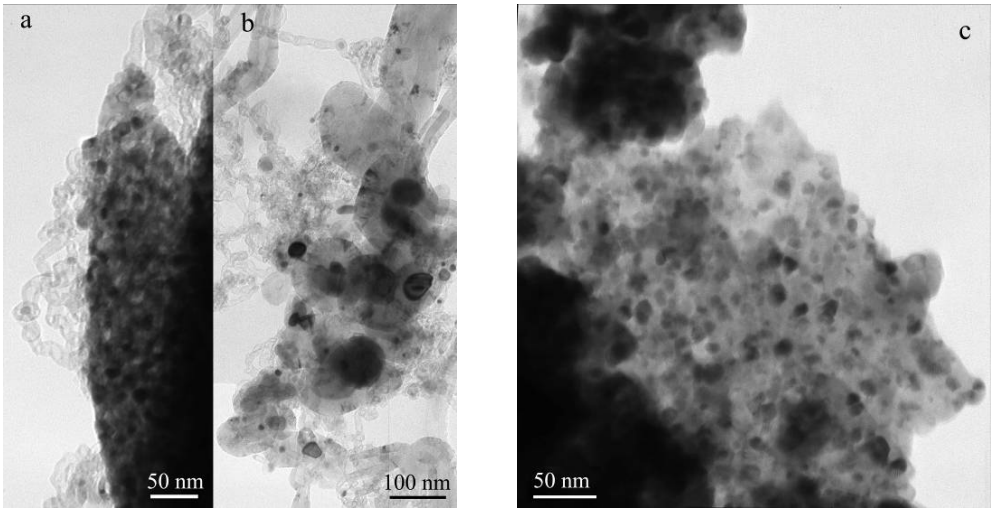

Fig. 5. TEM images of Ni sol–gel samples after long term test: (a) small Ni particles of $NiCe_{0.6}Zr_{2.97}$ (sg) incorporated in the support and inside thin nanotubes and (b) sintered Ni particles of $NiCe_{0.6}Zr_{2.97}$ (sg) separated from the support, encapsulated in carbon and thick nanotubes; (c) no sign of filamentous carbon on $NiCe_2Zr_{1.51}$ (sg). (Conditions: overnight reaction at 650 °C in $CH_4/CO_2 = 70/30$; total space velocity: 12 L h^{-1} g^{-1})

The surface carbon of these samples can be easily removed by O_2 (see the corresponding TPO curves in Figure 4). Since $NiCe_2Zr_{1.51}$ (sg) is less active and less stable in reforming reaction even with no filamentous carbon formation, its poorer catalytic performance should be more attributed to the partial reoxidation of nickel particles than to the carbon formation.

The impregnated Ni sample produced the highest amount of coke: carbon nanotubes of different diameters and encapsulating type carbon were seen after the reforming reaction (see Figure 6 a and b). The kinetics of carbon filament formation is well described in the literature[27,28]. We observed differently shaped Ni particles inside the nanotubes and Ni particles of more than 200-300 nm surrounded by graphitic shell of about 80 nm thickness (see Figure 6 a). Those were produced from the agglomerated Ni oxide particles already seen in as prepared state. Despite the very broad size distribution of this sample the catalytic stability is considerably higher than that of the sol-gel Ni samples, suggesting that large particles must be involved in the maintenance of long term activity.

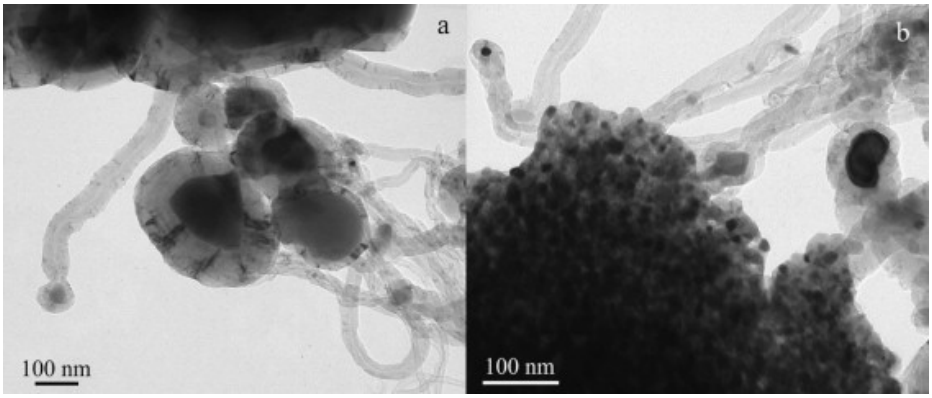

Fig. 6. TEM images of Ni/Ce_2Zr_2 (imp) after long term test: (a) Ni particles of 100–300 nm surrounded by graphitic shell and separated from the support and (b) support with smaller Ni particles inside carbon nanotubes (Conditions: overnight reaction at 650 °C in $CH_4/CO_2 = 70/30$; total space velocity: 12 L h^{-1} g^{-1}).

For the bimetallic sol-gel samples, the structural degradation and support segregation after catalytic run were even more pronounced. In the case of $NiCoCe_2Zr_{1.51}$ (sg), the EDS analysis during TEM measurement detected bimetallic 50-200 nm NiCo particles surrounded by thick encapsulating carbon together with the presence of thin nanotubes containing small Ni particles inside as in ref[29]. The sample $NiRhCe_2Zr_{1.51}$ (sg) looked somewhat similar to $NiCoCe_2Zr_{1.51}$ (sg) in TEM images. 100-150 nm size bimetallic NiRh particles and several large Ni particles were formed and encapsulated by graphitic shell, sit in the network of filamentous carbon. In both cases support segregation occurred to some extent as well, because almost pure ZrO_2 phase appeared which contained Ni according to EDS.

Considering the above observations and literature references[30], now we tend to describe TPO peaks obtained at high and low temperature to carbonaceous deposits of two distinctly different types in contact with distinctly different metal proximity. When small metallic particles in strong interaction with support being able to provide active oxygen are present and carbidic, amorphous or thin fragile filamentous carbon are formed, the TPO peak appears at lower temperatures, (or as in the case of the single TPO peak of Ni sol-gel samples). When sintered metal particles detached from the support are surrounded by graphitic robust nanotubes or thick rather encapsulating type carbon, TPO peaks are observed around 500-600^{o}C. The beneficial effect of Rh and Co addition is seen in the relative ease of oxidation of any kind of coke compared to the Ni samples that manifests itself in the decrease of TPO maxima. The other positive effect of Co and Rh might be the prevention of Ni oxidation and active alloy formation resulting in stable catalytic activity in the long term test. Encapsulating carbon is declared to cause deactivation, by blocking the metal surface[31], while beside of the formation of filamentous type carbon, even with a graphitic structure, catalyst can still work[32,33,34]. However, if the filamentous carbon formation is accelerated, eventually it is also detrimental causing catalyst plug-in, structural and metal particle destroy. For the increased formation of nanotubes metal particles should possess proper morphology in terms of exposure of open ⟨100⟩ and ⟨110⟩ and ⟨111⟩ crystal planes at the front and the back side, thus, for any reason "smoothened" metal particles produce less filaments but more amorphous carbon and Ni_3C or at high temperature shell-like encapsulating carbon[35, 36]. This can explain the reduced carbon formation on both NiCeZr (sg) samples, which do not contain large, faceted Ni, but rather small, partially oxidized Ni still incorporated in the oxide matrix.

Despite the fact that our catalyst are sintered, contaminated by all kinds of carbon, catalytic activity is extremely good concerning the reaction conditions (CH_4/CO_2=70/30) that are highly susceptible for coke formation. This indicates that carbon contamination may play a dynamic role in the reaction to produce CO in agreement with ref [5].

Alonso et al pointed out that broad particle size is even beneficial in catalytic point of view, because small particles causes CH_4 decomposition at the beginning of methane dry reforming, while large particles are responsible for long term stability due to the formation of non deactivating carbon deposits. The CO_2+C=CO (carbon gasification) reaction is structure sensitive favoured on small particles while the filamentous carbon formation is supressed[29]. This is in complete agreement with our results, since all the samples have broad particle size distribution after catalytic tests, and the samples that contain larger Ni or NiCo, NiRh particles exhibit more stable activity.

The $NiCe_{0.6}Zr_{2.97}$ (sg) sample was further investigated by X-ray photoelectron spectroscopy (XPS). In Figure 7 (1) the change of Ni 2p+Ce 3d spectra and (2) the C 1s region are plotted after in situ treatments In the "as prepared" state the nickel was in the form of Ni_2O_3 with 855.5 eV BE and the cerium in CeO_2 showing the characteristic satellite peak at 916.7 eV BE. After reduction with hydrogen, nickel oxide was mainly reduced to metallic nickel but about 30% of the nickel was still in the form of Ni^{2+}. The Ce^{4+} satellite practically disappeared

indicating the reduction of Ce^{4+}. The Ni/Zr atomic ratio, measured by XPS decreased from 0.098 to 0.059 and

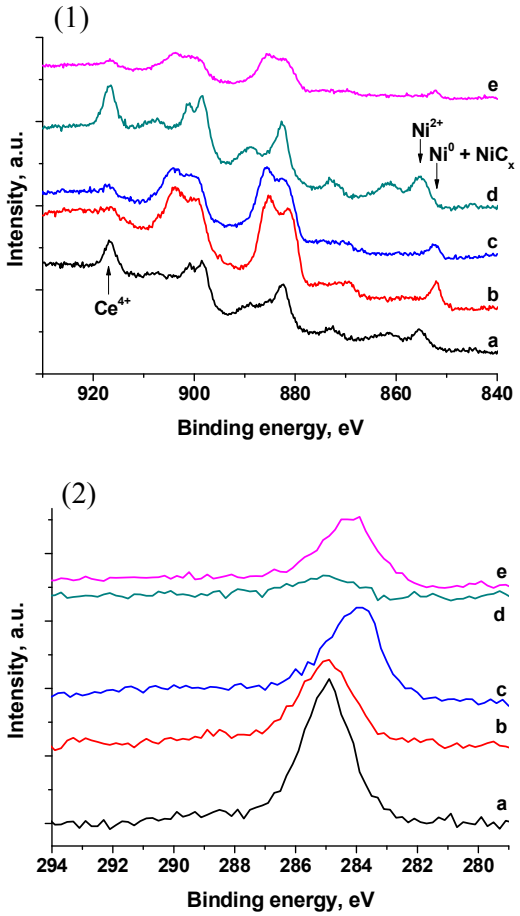

the surface carbon concentration decreased from 29.4 at% to 6.2 at%. We should note that by re-oxidation at room temperature with air, the initial Ni/Zr ratio was restored. This increase in the Ni/Zr ratio at room temperature is an indication of the mobility of nickel in the catalyst. CO_2+CH_4 reaction at 660°C had no influence on the shape of Ni, Ce and Zr spectra but carbon peak broadened and shifted to lower BE (see Figure 7(2)c). At the same time there was a decrease of about 4 eV in the charging of the sample, indicating an increased conductivity of the sample due to the carbonaceous layer. The "as prepared" state but with negligible amount of carbon could be regenerated by treating in air at 700°C (Figure 7(2)d). A second CO_2+CH_4 reaction returned the catalyst into the state as it was after the first reaction (Figure 7(2)c and 7(2)e). This suggests that the state of the catalyst adopts itself to the reaction conditions independent of the state (oxidized or reduced) before the reaction.

Fig. 7. (1) XPS spectra on $NiCe_{0.6}Zr_{2.97}$ (sg) sample: (a) as received, (b) after reduction in H2 at 770 °C/1 h, (c) after CO_2 + CH_4 reaction at 660 °C, (d) treatment in air at 700 °C/1 h and (e) after CO_2 + CH_4 reaction at 660 °C; (2) XPS spectra of carbon C 1s on $NiCe_{0.6}Zr_{2.97}$ (sg) sample: (a) as received, (b) after reduction in H_2 at 770 °C/1 h, (c) after CO_2 + CH_4 reaction at 660 °C, (d) treatment in air at 700 °C/1h and (e) after CO_2 + CH_4 reaction at 660 °C.

4. Investigations on $MgAl_2O_4$ supported systems

Compared to ceria, spinel $MgAl_2O_4$ oxide do not contain highly mobile lattice oxygen but is highly stable and thermally resistant, furthermore, it can ensure strong metal-support interaction with Ni. These are the main reasons why this oxide was chosen as a second support in our investigations.

Guo and co-workers experienced that the $MgAl_2O_4$ spinel layer formed in Ni/MgO-γ-Al_2O_3 can suppress the phase transition to form $NiAl_2O_4$[37]. Kiennemann and co-workers also used spinel and peroskvite supports [38, 39, 40, 41]. The authors found that $NiMg/Al_2O_3$ catalysts, prepared by co-precipitation method and Ni/MgO, prepared by impregnation, were effective dry reforming catalysts which was explained in terms of the reducibility and also of the good dispersion of Ni species. Further improvement was observed on the $LaNi_xAl_{1-x}O_3$ peroskvite materials prepared by sol–gel technique. The replacement of La by Ca, which has a lower ionic radius, favored a higher activity and stronger resistance to carbon deposition[42]. Filamentous coke was formed that was not harmful to the catalysts. The other issue, to modify the parent Ni

metal with a second metal was realized here by preparing Au-containing Ni catalysts using the spinel $MgAl_2O_4$ support, since we have a great experience in the preparation of mono and bimetallic AuPd, AuPt catalysts for other types of catalytic reactions. The addition of Au to improve the performance of Ni steam reforming catalyst via suppression of coke formation was already reported by others[43, 44, 45], however, to the best of our knowledge AuNi samples were not studied under dry reforming conditions. The effect of Au on coke formation was suggested to be similar to the ensemble control by sulphur[46]: at high sulphur coverage dissociation of methane is still possible but there are no more ensembles available for dissolution of carbon and nucleation of carbon whiskers.

According to the literature, large miscibility gap exist in the phase diagram of Au-Ni system[47]. There is a mutual solubility in the solid state above ~ 800°C, but at low temperature due to the large difference in atomic diameters of Au and Ni, they segregate and two distinct phases (rich in Au and rich in Ni) form, whose composition depends on the alloy composition and the temperature and the cooling rate. Despite the theoretical immiscibility of the two bulk metals at low temperatures, we can find several examples about the successful preparation of nanosize AuNi alloy or composite[48] nanoparticles which in most cases were found to possess synergetic interaction between Au and Ni[49, 50]. Unsupported AuNi particles were prepared by reduction of $AuCl_4$ and $NiCl_2$ with borohydride in the presence of SDS. After reduction at 850°C particle size was between d=10-100nm. XRD studies showed peak shift of Au due to the inclusion of Ni atoms. TEM observed big contrasts between particles, which meant that Au-based and Ni-based systems coexisted, however, after heat treatment more uniform contrast was observed, meaning that Au and Ni formed probably alloys[50].

We can see that mixing Ni with Au and application this combination for dry reforming catalyst are of great challenges, moreover, this research topic has not been deeply investigated yet. In the next part of the work we report our results on trying to elucidate the role of gold in methane dry reforming using Au containing $Ni/MgAl_2O_4$ catalysts. Studying monometallic Ni samples, the role of various carbon species formed on the $MgAl_2O_4$ – supported catalyst' surface during the reaction is also shown. Different synthesis routes, impregnation and sol method were applied as preparation techniques. Gold and Ni content of the samples varied between 0-10 wt%, depending on the preparation. Since metal content influences major catalyst parameters (for example dispersion, distribution of Au and Ni), we can compare the different samples only with special care.

4.1. Structure and catalytic behaviour of Ni, $NiAu/MgAl_2O_4$ catalysts prepared by impregnation

First, we followed the process described elsewhere[44] when preparing monometallic 8 wt%Ni or 0.5wt%Au8%Ni/$MgAl_2O_4$ solely by impregnation. The most important to point out here is that Ni was calcined and reduced before impregnation with Au precursor and no further reduction treatment was done before the first catalytic tests. The results of this work have been already published, so we will highlight only the most important outcomes focusing on the structural characterization of carbon deposits.

In Figure 9 the CO_2 conversion in the first reaction for 8%Ni/$MgAl_2O_4$ and 0.5%Au-8%Ni/Al_2O_4 samples and that of the corresponding calcined samples are plotted. The results obtained in the temperature programmed reaction suggested that the presence of gold retards the catalytic dry reforming reaction. We have to pay attention to the behavior of calcined samples: after a threshold temperature the reaction abruptly started and finally reached 100% CO_2 conversion. We can deduct that without hydrogenation the active bulk nickel component remains in oxidized state and at around 650 °C some reduction occurs to form metallic nickel and the reaction starts and is completed with high rate. The reduction might be induced directly by the methane itself or in the long induction period the CO and H_2 formed in small amount

can reduce the surface of the Ni. For calcined NiAu the reaction starts at around 600 °C and smoothly increases up to full conversion that is explained by the presence of Au promoting reduction of oxidized Ni. During overnight reaction over $Ni/MgAl_2O_4$ both CO_2 and CH_4 conversion decreased, while $AuNi/MgAl_2O_4$ sample exhibited a more stable performance.

In Figure 10 a representative TEM image of as prepared $AuNi/MgAl_2O_4$ sample is presented. The size of gold particles is fairly large while the nickel particles are small (d<10 nm) in size. Alloy formation could not be excluded but direct evidence was not available from the TEM measurements.

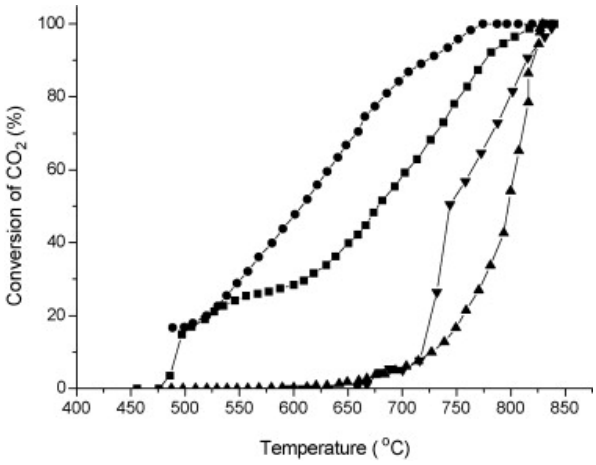

Fig. 9. Comparison of $Ni/MgAl_2O_4$ and $NiAu/MgAl_2O_4$ catalysts in $CO_2 + CH_4$ in first reaction (● and ■, respectively) and after TPO (□ and □, respectively).

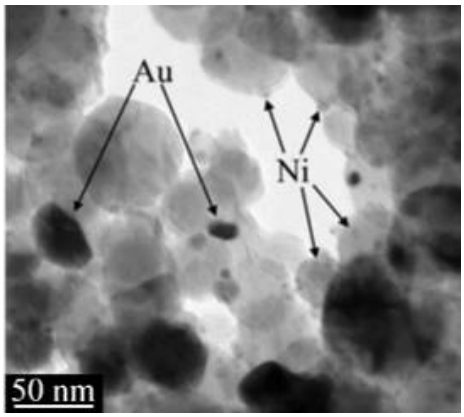

Fig. 10. TEM image of as prepared $0.5\%Au8\%Ni/MgAl_2O_4$

TPO was carried out in order to evaluate the carbon deposition on the catalyst surface. For $8\%Ni/MgAl_2O_4$ the TPO peaks were centered at 650 and 680 °C and the highest amount of carbon was determined after the first reaction (44 mg). After the second reaction the amount of carbon recovered decreased (18.4 mg). After the overnight time-on-stream test it decreased to a surprisingly low level (ca. 4 mg). In the case of $NiAu/MgAl_2O_4$ the carbon deposit was bonded to the surface a little stronger than on the nickel sample (higher temperature of peak maximum), although the surface carbon recovered after the first reaction was somewhat smaller (31 mg carbon). The major difference between the two samples was in the amount of carbon deposit after the overnight reaction: while on the bimetallic sample there was only a minute drop in the amount of carbon deposit, on $Ni/MgAl_2O_4$ there was a drastic decrease in the recovered carbon between the first and overnight reaction of dry reforming. This suggests that part of the carbon was continuously removed during long term run in the case of monometallic Ni sample.

In Figure 11 the XRD patterns are presented for $Ni/MgAl_2O_4$. Curve A shows that the prevailing spectrum is assigned to the magnesium aluminum spinel structure and only a small amount of metallic Ni appears at 52°. After first reaction small amount of graphite appeared at 26° with parallel to the increased Ni line (spectrum B). After long time on stream the graphite is further increased (line (C). Spectrum D proves that after calcination crystalline graphite disappears and Ni is oxidized. In the case of gold promoted sample the major difference to the Ni-only sample is that after long term test there was no graphite formation. On the bases of XRD there was no indication for bulk Au–Ni alloy formation, but it may not be excluded especially on the surface, because the peaks of the support overlap with the peaks of Au.

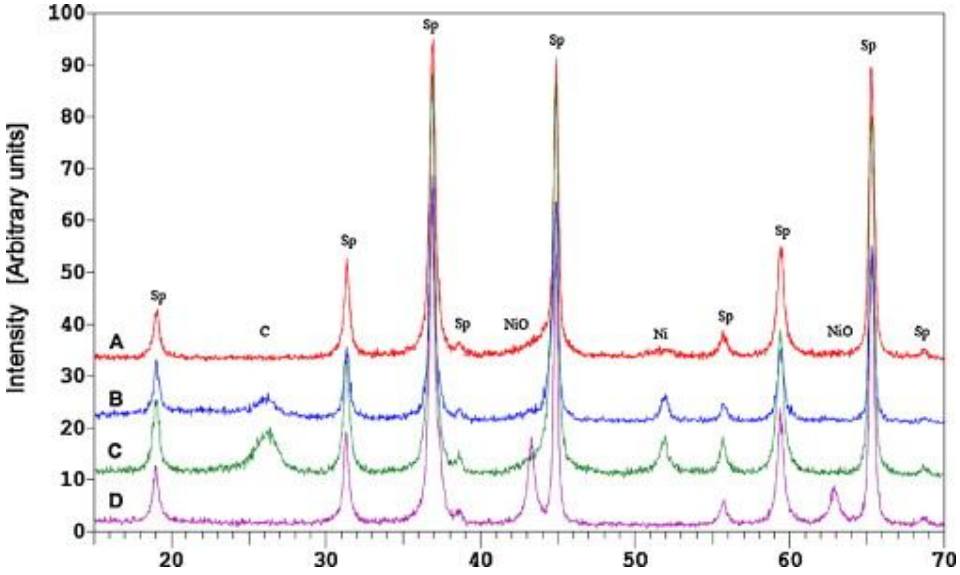

Fig. 11. XRD diffraction patterns of 8%Ni/$MgAl_2O_4$ sample. (A) Before reaction, (B) after first reaction, (C) after overnight reaction, and (D) after TPO.

XPS spectra of Ni/$MgAl_2O_4$ sample after different treatments in the C 1s and Ni 2p region are given in Figure 12 a and b, respectively. The assignments[51, 52] of the fitted components of carbon species are hydrocarbons and adventitious carbon at 285 eV, oxidized carbon at 289 eV, carbide in NiC_x at 282 eV.

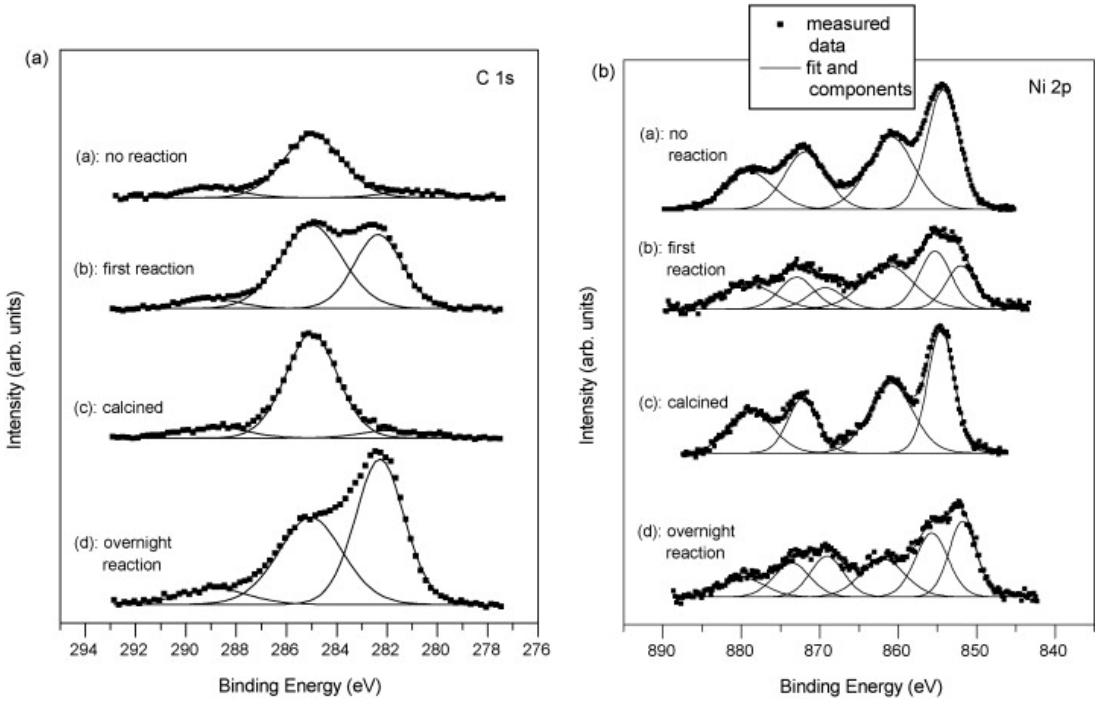

Fig. 12. (a) XP spectra of Ni/$MgAl_2O_4$ sample in C 1s core level region: (a) before reaction, (b) after first reaction, (c) after calcination, and (d) after overnight reaction. (b) XP spectra of Ni/$MgAl_2O_4$ sample in Ni 2p core level region (a) before reaction, (b) after first (single) reaction, (c) after calcination, and (d) after overnight (multiple) reaction.

The nickel carbide cannot be distinguished from Ni^0 by the Ni 2p spectra alone because there is minute difference in the binding energies. The binding energy for Ni^0 and NiC_x is the same at 852 eV. The reason why Ni^0 is not visible in the sample by XPS before reaction is that during transfer of the reduced sample in air (after initial treatment) Ni^0 would be oxidized to Ni^{2+} uppermost 6–10 Ni layers (Ni_2O_3 at 855 eV and the satellite for Ni_2O_3 at 861 eV). In contrast, the XRD can identify Ni^0 because it measures the whole bulky nickel which contains mainly Ni^0 species. The catalyst sample measured by XPS after the first reaction cycle contains nickel carbide (NiC_x) and Ni_2O_3 evidenced both in the Ni 2p and C 1s spectra. On regeneration of the catalyst by oxygen treatment the nickel carbide is removed and the XP spectra are the same as the ones of the fresh catalyst. However, after overnight reaction the activity of the catalyst decreased and the XP spectra show a substantial increase in the carbide peaks together with a decrease in the surface Ni concentration indicating that carbon is covering mainly the Ni component. When the reaction is repeated several times the XPS peak increases (Figure 12a curves (b) and (d)).

Now we can conclude based on the above results that the CO_2 conversion of the reaction was complete at 800 °C for both Ni and NiAu catalysts although 0.5 wt% gold hampered the dry reforming measured in temperature programmed reaction, whereas on long range the activity was a bit improved in the presence of gold. Concerning the role of surface carbon, it was established that on $Ni/MgAl_2O_4$ in sequential reactions the catalyst was deactivated by graphite like carbon deposit and carbon nanotubes (CMWNT) measured by XRD and TEM, while XPS revealed the formation of Ni carbide which was not observable by other techniques. On the catalyst containing gold no crystalline graphite or CMWNT were produced. The first step of carbon deposition is the formation of amorphous NiC_x which is transformed into graphite shell or CMWNT. This last step was significantly retarded by gold in the bimetallic sample.

Unfortunately, when we repeated the preparation to get a new batch of sample from a new bottle of Ni-nitrate hexahydrate (because the first batch was over), the prepared samples behaved in a different way: the monometallic Ni and the NiAu sample were of similar activity and Ni performed better in the durability test, in contrast with the previous results. The reason for this is unknown for us at the moment. Moreover, when 3% gold was introduced instead of 0.5 wt%, carbon deposition increased. We should remember, that alloying of Au and Ni was not seen by TEM, although the effect of gold on the properties of Ni catalyst was evident (differences in activity and coke formation), but the observed differences must have been caused by differences in Ni dispersion and in composition or distribution of AuNi alloy if any was present. These experiences governed us to the application of sols, since it is a more controllable way of preparation than impregnation, and because the contact of bulk immiscible Au and Ni phases during a fast liquid phase reduction was thought to happen more easily.

4.2. Formation, structure and catalytic behaviour of Ni, $NiAu/MgAl_2O_4$ prepared by sol method

We have some experience in application of precious metal sols for catalytic purposes. Different reducing and stabilizing agents allow one to get particle size in desired range and if proper interaction is provided between the stabilized nanoparticles and the support surface added to the system, adsorption takes place and one gets the supported sample after filtering, drying and calcination.

We tried to adopt the sol method to produce Ni or AuNi nanoparticles with Ni core, Au shell. The usual reducing agents, tannin and citrate were not strong enough to reduce Ni(II) nitrate, moreover, the slightly basic pH that was used with these reducing agents for Au sols, resulted in precipitate, probably Ni-oxyhydroxide formation. Finally, at lower pH, in the presence of more tannin and citrate, $NaBH_4$ was successfully used to reduce Ni(II) ions at 60^oC. Addition of $HAuCl_4$ solution was done after 9 min of addition of Ni-nitrate and

immediate reduction of Au took place. Our aim was to deposit Au on the surface of Ni particles but we can not exclude that separate phase formation took place as well, producing individual Au particles beside core-shell structured NiAu. After 30 min at 60°C the adsorption of nanoparticles onto the $MgAl_2O_4$ support was carried out with the aid of a polycation (PDDA). The as prepared catalysts were calcined at 550 °C to remove the carbonaceous contamination. During Ni reduction we observed a color change to deep brownish-grayish that turned a bit reddish while adding Au^{3+} ions. However, fast fading was observed with time and after 1-2 hours the pure Ni sol was greenish, meaning that dissolution of Ni must happened.

Figure 13 depicts the TEM images of a) parent Ni sol before addition of Au precursor and b) the Au containing counterpart. The size of the individual particles in the Au-Ni sol is smaller than the starting size of Ni particles, supporting the occurrence of Ni dissolution. According to the elemental analysis, the supported samples contained indeed less Ni than the nominal, 10 wt% value. Metal content and particle size of the samples can be seen in Table 2. The Ni loading of the samples was 4-5 wt%, while Au content was different but agreed with the nominal values. The sample abbreviations reflect the Au content in wt%. The particle size after catalytic run with the usual temperature ramp increased with Au content which could be suspected from the uneven distribution of Au already in liquid phase acting as a kind of chemical glue that connects particles together (see Figure 13 b).

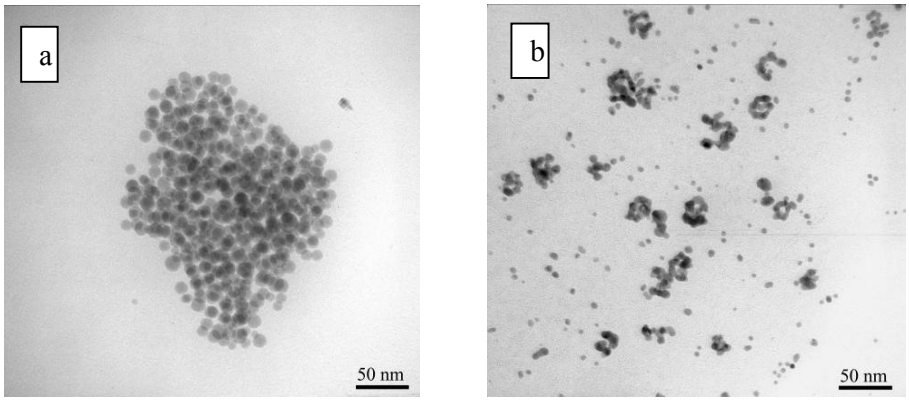

Fig. 13. TEM image of a) parent Ni sol and b) NiAu3 sol (EDS on the larger ensembles of particles gives higher Au signal than on the separated ones)

Table 2. Metal content of the sol samples and particle size determined by TEM after DRM reaction

Sample name	Me content		Ni/Au	d_{Me} (nm) after reaction (TEM)
	Ni wt%	Au wt%		
Ni_sol	4.1[a]			6.7±4.6
NiAu**0.45**_sol	4.2[a]	**0.45**[c]	30	8.6±9.1
NiAu**1.4**_sol	4.9[a]	**1.4**[c]	10	9.6±5.8
NiAu**3**_sol	4.1[a]	**3**[b]	5	-

a: measured by XRF, b: nominal, c: measured by PGAA

The temperature programmed reduction of the calcined samples was done in repeated cycles to mimic the regeneration step in between catalytic testreactions. (After the first catalytic run the samples were calcined at 650-700°C and reduced at 750°C which meant the regeneration step.) The cycles of the two TPR measurements and the corresponding imitated catalyst treatments were as follows:

1. calcination at 550°C ~ initial calcination pretreatment before reaction
2. TPR 1 (full symbols) ~ initial reduction pretreatment before reaction
3. second calc. at 650°C ~ oxidation of deposited carbon (and NiO formation)
4. TPR 2 (empty symbols**)** ~ reduction step to get active catalyst again

In Figure 14 it is clearly seen that only one peak appears at ~440°C in TPR2 of NiAu sol samples while still two wide peaks can be seen for the monometallic Ni sample. Dispersion is not the main parameter to influence reducibility of the samples, because as it is shown in Figure 14 b, the mean particle size and the size distribution is shifted with increasing Au content but the peak position and area does not change. Moreover, there is not a big difference between the size of Ni/metal in the monometallic and bimetallic samples. We rather believe that with the repetition of heat treatments and especially H_2 treatment, Au redistribution happens resulting in more homogeneous arrangement of Au and Ni that is manifested in a single reduction peak during second TPR run.

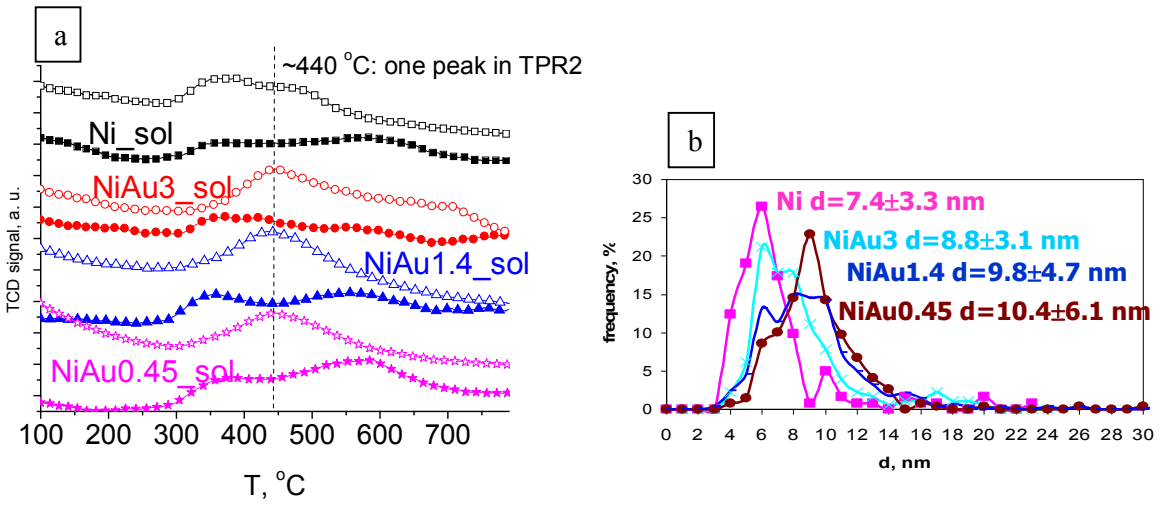

Fig. 14. a) TPR curves of the sol samples. Emty symbols correspond to the TPR2 cycle (see text above) and b) Particle size distribution of sol samples determined by TEM after the TPR cycles.

Catalytic activity of the sol samples was measured both in temperature programmed way and during long term run at 650°C. The results are shown in Figure 15. Au addition induced again a delay in the starting temperature as in the case of impregnated sample (see previous chapter) and 100% CO_2 conversion was reached at lower temperature than in the case of Ni_sol. However, the bimetallic samples in the second run after regeneration exhibited decrease in activity (not shown here), while Ni_sol sample did not lose its original activity. This means that a kind of structural rearrangement of NiAu samples happened during the first reaction followed by regeneration that caused irreversible deactivation (bulk AuNi alloy formation?). Here we should recall the TPR results that also suggested structural changes in/before the regeneration step (the one peak in TPR2).

There is another eye-catching issue in the activity curve of the bimetallic samples: the reaction starts abruptly at higher temperatures (especially at higher Au content), while product appearance/formation starts smoothly in the case of Ni_sol sample. This is consonant with the sudden jumps seen when only calcined (not reduced) Ni samples (both on $MgAl_2O_4$ and Ce-Zr-oxide) were tested in the reaction. In those cases the surface of Ni must have got reduced in order to commence the reaction. Here, in the case of NiAu sol samples, we speculate that in spite of the previous reduction treatment there is not enough Ni species on the surface (particles are still covered by Au atoms) and a certain temperature (~500°C) is required for Ni to diffuse to the surface of particles and then the reaction sets in. This assumption is based on a few literature references as well, that describe and calculate the surface segregation in model AuNi alloys and the restructuring of this alloys as temperature increases[53,54].

The long term stability (Figure 15 b) of samples is also influenced by gold: the best sample is the monometallic Ni with very stable performance and high conversions (after a slight initial

deactivation), while bimetallic samples are worse. Carbon contamination, the type and the amount of carbon deposits or the instability of AuNi surface or bulk alloy must be the reasons for this behaviour rather than sintering. The CO/H_2 ratio determined decreases with increase of Au content.

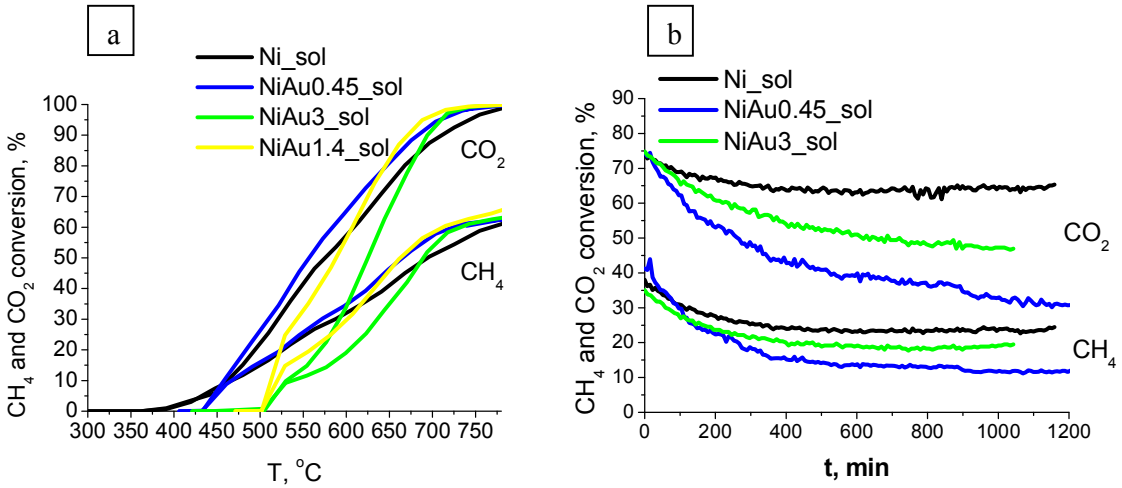

Fig. 15. a) Catalytic activity of sol samples in the first reaction and b) Long term stability results measured at 650 °C. CO/H_2 ratios are 1.0, 0.9 and 0.75 for Ni_sol, NiAu0.45_sol and NiAu3_sol respectively.

Finally, let us report on the carbon deposits removed during TPO measurements. Figure 16 shows the TEM image of NiAu0.45_sol after the second catalytic run. We can see 20-25 nm sized metal particle containing both Au and Ni inside thin nanotubes and small d<10 nm metal (Ni, Au or NiAu) particles sitting on the support. TPO curves in Figure 16. b ascertain again that Au addition at low concentration might increase and at higher loading decrease the amount of carbon deposit. The decreased amount of coke in the temperature programmed reaction forms on the surface of a less effective catalyst with 3wt% Au (NiAu3_sol), but the same catalyst performs better in the long term run and produces only 0.5 mg carbon at 650°C compared to the sample that contains only 0.5wt% Au. (The recovered amount of coke after long term run is very high (24 mg) for NiAu0.45_sol, low for NiAu3_sol (0.5 mg) and moderate (4.1 mg) for the monometallic Ni_sol sample.) In general, coke is more difficult to remove from the bimetallic sol samples than from Ni_sol sample (see the shift of peak maxima with increase of Au content), as in the case of impregnated $0.5\%Au8\%Ni/MgAl_2O_4$ sample (see previous section).

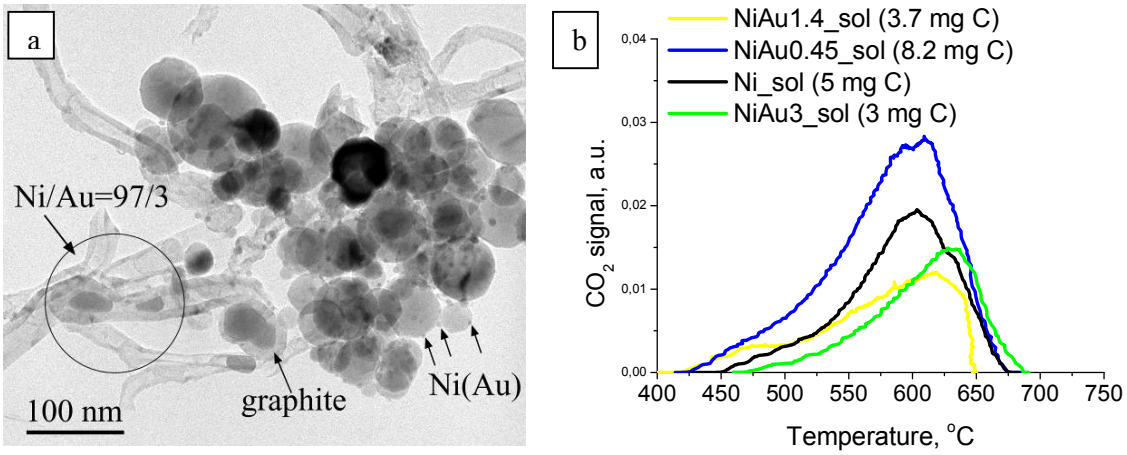

Fig. 16. a) TEM image of NiAu0.45_sol after the second DRM reaction. Ni/Au ratio was determined by EDS. and b) TPO curves obtained after the first DRM reaction and the amount of carbon removed.

The observed differences between the AuNi samples may reflect the different distribution and stability of (surface) bimetallic phases that seemed to change during the high temperature pretreatments (TPR results) and during the catalytic reaction as temperature increased and also with time on stream.

4.3. The effect of gold in dry reforming: still a question

Considering the above results we are still not able to give clear determination how gold modifier acts on dry reforming activity and coke formation. The overall Au-Ni catalyst system seems extremely sensitive to parameters such as temperature, dispersion of Ni, Au content, etc. Ideal catalyst with monodisperse particles and even distribution of Au in/on the Ni particles would help to answer all the questions. Sol preparation method can be a good choice for such purpose but the synthesis parameters must be further optimized (to get uniform coverage of Au on Ni). We should not forget that this research topic is not thoroughly investigated, indeed there are no publications - to the best of our knowledge- that report on methane dry reforming carried out with Ni-Au catalyst. However, there are a few literature references dealing with steam reforming on NiAu systems, as follows.

It is widely accepted that steam reforming and graphite formation over Ni catalysts are structure sensitive. Step sites are considerably more reactive than close-packed facets for both reactions. Nucleation of graphite should start at steps of Ni particle and graphene (one-atom-thick planar sheets of graphite) is the most stable form of carbon on Ni(111) and so there is a driving force for graphene formation. DFT calculations showed[45] that Au atoms are also located on the surface step sites of 3.5 nm Ni particle (when Au concentration is 2 atomic %) even at high temperature. Therefore, this was suggested as the main reason for the suppression of graphite formation observed for these systems. EXAFS spectra obtained on a real 1.7wt%Au9.6wt%Ni/$MgAl_2O_4$ catalyst after reduction at 550 ^oC agreed well with the simulated curve representing that 44% of the total Au is in the form of NiAu surface alloy and 56% is present as separate bulk Au particles, but the particle size was assumed 2 nm for the simulated curve. It was admitted that particle size distribution, possibly adsorbed gases and metal-support interactions were not included in the calculations. King and co-workers[44] added 0.1-1wt% Au by impregnation to a previously calcined, reduced and passivated 8.8 wt%Ni/$MgAl_2O_4$ catalyst applied in n-butane steam reforming. By addition of gold, EXAFS measurements showed a significant Au–Ni nearest neighbor interaction when the Ni component was in the reduced state and Au≤0.2 wt%. At higher concentrations, Au segregation happened. XANES analysis revealed transfer of electronic charge from Au to Ni as a result of surface alloy formation. Au modification decreased the number and the reactivity of surface sites (H_2 chemisorption and N_2O TPD experiments). Moreover, presence of Au suppressed coking (both the coking rate and the total amount of coke deposited after 500 min) during n-butane steam reforming between 450-550^oC: most effectively at 450^oC and to a decreasing extent with increasing temperature. In methane steam reforming at 550^oC lower initial activity and lower deactivation rate was observed in the case of 0.4%Au8.8%Ni/$MgAl_2O_4$ sample but carbon content was not given.

In methane reforming with CO_2 the temperature is increased up to 700-800^oC, and all the above statements and suggestions valid for steam reforming at lower temperature can fail to describe the prevailing conditions of dry reforming. Moreover, our results on impregnated and sol-prepared samples may seem a bit contradictory as we come to the discussion of gold effect. In our opinion, it is a very complicated task to solve all the questions with such amount of work and experiments we did. The only agreement between all the samples that CO_2 peak during TPO of deposited carbon appears at higher temperature on Au-contaning samples. The other characteristics, viz. the amount of carbon deposit and the activity order compared to the pure Ni samples exhibit wide variety, but generally monometallic Ni samples are more active. To completely clarify the ongoing surface reconstructions of NiAu systems, that are very

sensitive to the catalyst composition and temperature, more experiments and sophisticated in situ characterisation techniques are needed. This will be realised in the future as a continuation of this work. If we are able to control the AuNi alloy properties and stability under dry reforming condition, and balance the activity and coke formation, the addition of Au may be even favourable.

5. Methane decomposition followed by reverse Boudouard reaction for carbon removal

Finally in order to elucidate part of the surface elementary processes, pure methane decomposition (without CO_2) was studied on both Ce-Zr-oxide and $MgAl_2O_4$ supported Ni catalysts. In Figure 17 the original mass spectra are seen, where m/z=2, 16, 18, 28 and 44 corresponds to hydrogen, methane, water, carbon monoxide and carbon dioxide, respectively. (For some set up error, the hydrogen signal is out of range in spectrum b in between 450-600°C.)

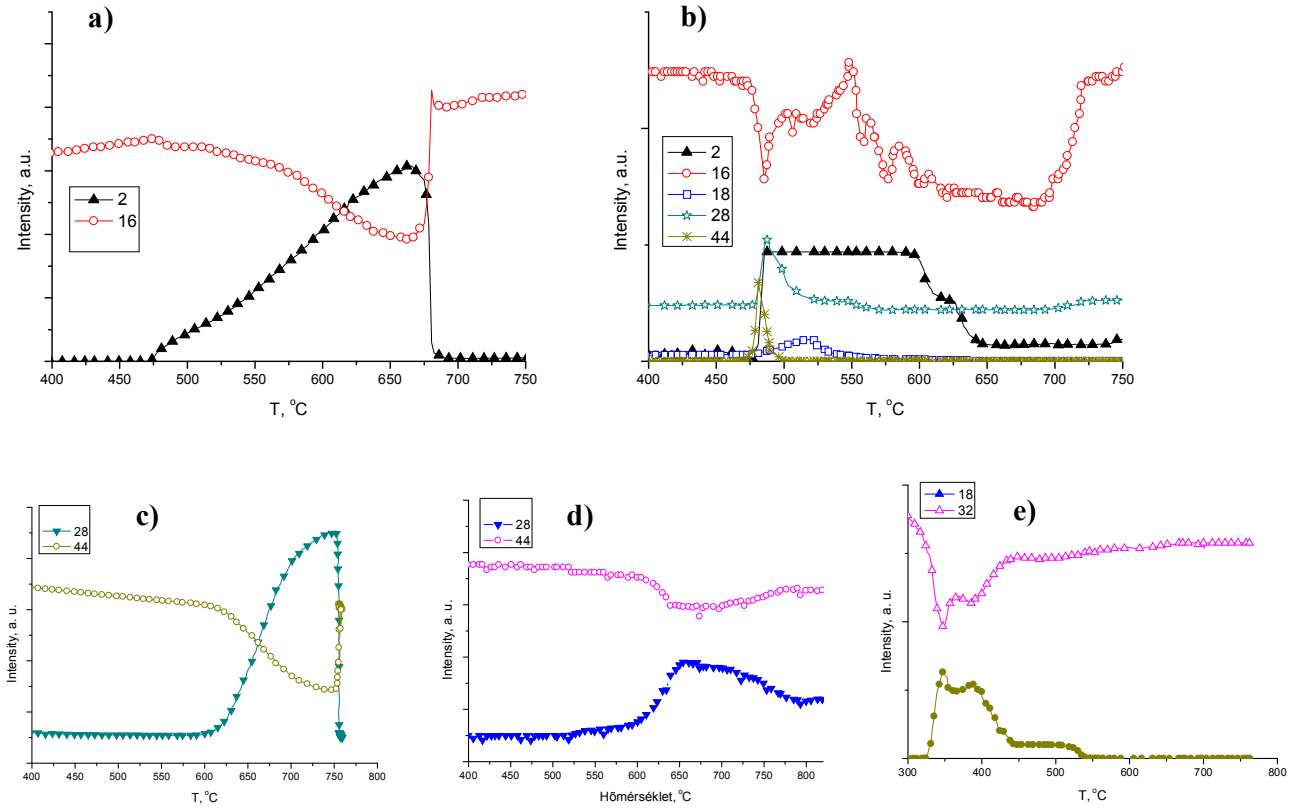

Figure 17. Temperature programmed decomposition of CH_4 on a) 8%Ni/$MgAl_2O_4$ and b) on $NiCe_{0.6}Zr_{2.97}$ (sg). TPO curves: CO_2-TPO of the deposited carbon on c) 8%Ni/$MgAl_2O_4$ and on d) $NiCe_{0.6}Zr_{2.97}$ (sg) and O_2-TPO of the deposited carbon on e) $NiCe_{0.6}Zr_{2.97}$ (sg).

During methane decomposition experiments up to ~450°C no products are formed, then CO and water are measured in the case of sol-gel sample while only hydrogen and minute amount of water (not shown here) is detected for Ni/$MgAl_2O_4$, see curves b and a, respectively. Since there is no oxygen source present in the gas phase, most likely some amount of oxygen is taken from the easily removable oxygen in Ce-Zr-oxide, since the sample was oxidized before the experiment. There is no such active oxygen available on $MgAl_2O_4$. The decomposed methane leaves carbonaceous deposit on the surface. As shown in Figure 17 c) and d), this carbon can be removed from both catalysts by CO_2 due to the occurrence of reverse Boudouard reaction

above 600°C. With O_2, the same type of deposited carbon originating from methane is easily removed on Ce-Zr-oxide supported sol-gel Ni sample well under 600°C, as spectrum e) shows. Józwiak et al. studying $NiRh/SiO_2$ detected graphitic carbon formation (by XRD) but the catalyst was active and stable. This carbon could be partially gasified by CO_2, although the subsequent O_2-TPO removed the remaining carbon from the catalyst[55]. In our case after CO_2 treatment, the TPO with O_2 (not shown) could not remove further coke from the sample in the case of $NiCe_{0.6}Zr_{2.97}$ (sg) but minor amount of CO_2 formed in the same type of experiment when $Ni/MgAl_2O_4$ was tested.

These results also reflect that the Ce-Zr-oxide itself (in contact with Ni) has significant role in oxidation of coke.

6. Summary

We developed new Ni-based catalysts with nanosized particles stable at high temperature for longer time and fairly tolerant to the presence of deposited carbon. As support either thermostable $MgAl_2O_4$ was chosen, because it was expected to stabilize higher metal dispersion by strong interaction with the active phase; or Ce-Zr-oxides were applied, which are able to provide highly mobile oxygen species to remove surface coke formed. Metallic or bimetallic sites were formed by a) sol-gel process (Ni, NiCo and NiRh/Ce-Zr-oxides); b) traditional impregnation ($Ni/MgAl_2O_4$, Ni/Ce-Zr-oxides) and c) a newly developed sol-method (Ni and $AuNi/MgAl_2O_4$). Sol-gel method was expected to integrate nickel into the oxide framework, thus hindering metal sintering, sol method was chosen to ensure close contact of bulk immiscible Au and Ni phases and control small particle size, while impregnation was used as reference. The effect of the second metal (Co, Rh, Au) on catalytic performance and on coke deposition was investigated using selected supports. It was established that

a) If Ni is built in a CeZr-oxide structure by sol-gel technique, the small size of nickel can be better maintained and the carbon formation is dramatically decreased compared to the case when Ni was impregnated on the same type of support, because the proximity of oxide and the finely dispersed Ni facilitates carbon gasification. However, sintered, more robust metallic or bimetallic particles seem to be important in long term stability.
b) On impregnated $8\%Ni/MgAl_2O_4$ sample in sequential reactions the catalyst was deactivated by encapsulating type carbon (graphite shell) and carbon nanotubes detected by XRD and TEM, while XPS revealed the formation of Ni carbide which was not observable by other techniques. The presence of gold introduced by impregnation retarded the catalytic dry reforming reaction.
c) Using nickel catalyst prepared by sol technique on $MgAl_2O_4$, the amount of surface carbonaceous deposits could be decreased due to high dispersion of stable metal sites. Small amount of Au increased the carbon deposited in methane dry reforming, while 3wt% Au decreased it compared to the pure $4\%Ni/MgAl_2O_4$ sample which exhibited the best activity and stability. However, carbon content and activity are not in straightforward relation. Significant restructuring of AuNi particles prepared by sol method is suggested to happen during oxidation/reduction treatment and during catalytic run (based on the catalytic and TPR results).

It is very difficult to compare all the catalyst systems, because they were different in terms of dispersion, metal content and type of support. In general, the best catalyst must be able to balance between advantageous carbon formation and carbon gasification on the surface, while keeping the metal sites small and in zero oxidation state during the reaction. This is achieved the most by the $Ni/MgAl_2O_4$ sample prepared by sol-method.

The mechanism of coke formation depending on several parameters will be studied in a static circulation system that will be used with ^{13}C-labeled reactants in the near future. Thus,

we will be able to see what the source of coke is and how this source changes with temperature or catalyst structure or etc.

References

1 M. C. J. Bradford, M. A. Vannice, Catalysis Reviews Science and Engineering 41 (1999) 1

2 L. Guczi, G. Stefler, O. Geszti, I. Sajó, Z. Pászti, A. Tompos and Z. Schay, Appl. Catal., 375 (2010) 236–246

3 M.-S. Fan, A. Z. Abdullah, S. Bhatia, ChemCatChem 1 (2009) 192-208

4 Darujati A.R.S., Thomson W.J., Chemical Engineering Science, 61 (2006) 4309

5 N. A. Pechimuthu, K. K. Pant, S. C. Dhingra, Industrial and Engineering Chemistry Research, 46 (2007) 1731-1736

6 F. Pompeo, N. N. Nichio, A. A Ferretti, D. Resasco, Int. J. of Hydrogen Energy 30 (2005) 1399-1405

7 S. Therdthianwong, A. Therdthianwong, Ch. Siangchin, S. Yongprapat, J. Hydrogen Energy 33 (2008) 991–999

8 M. Rezaei, S.M. Alavi, S. Sahebdelfar, Liu Xinmei, Ling Quian, Zi-Feng Yan, Energy & Fuel 21 (2007) 581-589

9 M. Rezaei, S. M. Alavi, S. Sahebdelfar, X. Liu, P. Bai, Z.-F. Yan, Applied Catalysis B 77 (2008) 346–364

10 M. Rezaei, S.M. Alavi, S. Sahebdelfar, Z.-F. Yan, Materials Letters 61 (2007) 2628–2631

11 S. Corthals, J. Van Nederkassel, J. Geboers, H. De Winne, J. Van Noyen, B. Moens, B. Sels, P. Jacobs, Catal. Today 138 (2008) 28-32

12 C. E. Daza, C. R. Cabrera, S. Moreno, R. Molina, Appl. Catal. A., 378 (2010) 125-133

13 C. E. Daza, J. Gallego, F. Mondragón, S. Moreno, R. Molina, Fuel 89 (2010) 592-603

14 J. A. Montoya, E. Romero-Pascual, C. Gimon, P. Del Angel, A. Monzón, Catal. Today 63 (2000) 71-85

15 J. C. Vargas, E. Vanhaecke, A.C. Roger, A. Kiennemann, Studies in Surface Science and Catalysis 147 (2004) 115-120

16 F. Romero-Sarria, J. C. Vargas, A. C. Roger, A. Kiennemann, Catalysis Today 133-135 (2008) 149-153

17 E. Ambroise, PhD thesis, Strasbourg 2010

18 B. Koubaissy, A. Pietraszek, A.C. Roger, A. Kiennemann, Catal.Today doi:10.1016/j.cattod.2010.01.050

19 M. R. Goldwasser, M. E. Rivas, E. Pietri, M. J. Pérez-Zurita, M. L. Cubeiro, L. /Gingembre, L. Leclercq, G. Leclercq, Applied Catalysis A, 255 (2003) 45–57

20 Gustavo Valderrama, A. Kiennemann, M. R. Goldwasser, Catal. Today 133–135 (2008) 142–148

21 German Sierra Gallego, Catherine Batiot-Dupeyrat, Joel Barrault, Elizabeth Florez, Fanor Mondragon, Appl. Catal. A., 334 (2008) 251–258

22 D. Chen, R. Lodeng, A. Anundskas, O. Olsvik, A. Holmen, Chem. Eng. Sci 56 (2001) 1371-1379

23 V. A. Tsipouriari, A. M. Efstathiou, X. E. Verykios, J. Catal. 161 (1996) 31-42

24 M. A. Goula, A. A. Lemonidou, A. M. Efstathiou, J. Catal. 161 (1996) 626-640

25 D. Chen, R. Lodeng, A. Anundskas, O. Olsvik, A. Holmen Chem. Eng. Sci 56 (2001) 1371-1379

26 X. Junke, Z. Wei, W. Jihui, L. Zhaojing, M. Jianxin, Chinese J. Catal. 30(11) (2009) 1076-1084

27 J. W. Snoeck, G. F. Froment, M. Fowles, J. Catal. 169 (1997) 240-249

28 L. A. Avdeeva, T. V. Reshetenko, V. B. Fenelonov, A. L. Chuvilin, Z. R. Ismagilov, Carbon 42 (2004) 2501-2507

29 D. San-José Alonso, J. Juan-Juan, M. J. Illán-Gomez, M. C. Román-Martínez, Appl. Catal. A: Gen. 371 (2009) 54-59

30 W. Pan, Ch. Song, Catal. Today, 148 (2009) 232-242

31 W. Gac, A. Denis, T. Borowiecki, L. Kepinski, Appl. Catal. A: Gen. 357 (2009) 236-243

32 G. Carneiro de Araujo, S. Maria de Lima, J. M. Assaf, M. A. Pena, J. L. Garcia Fierro, M. do Carmo Rangel, Catal. Today 133-135 (2008) 129-135

33 Y. Zhang, K. J. Smith, J. Catal. 231 (2005) 354-364

34 M. Matsukata, T. Matsushita, K. Ueyama, Chem. Eng. Sci. 51 (1996) 2769-2774
35 F. Frusteri, L. Sparado, F. Arena, A. Chuvilin, Carbon 40 (2002) 1063-1070
36 X. Zhu, P. Huo, Y. Zhang, D. Cheng, C. Liu, Appl. Catal. B: Environmental 81 (2008) 132-140
37 J. Guo, H. Lou, H. Zhao, D. Chai, X. Zheng, Appl. Catal. A: Gen. 273 (2004) 75-82
38 M. Parvary, S.H. Jazayeri, A. Taeb, C. Petit, A. Kiennemann, Catal. Commun., 2 (2001), pp. 357–362
39 A. Djaidja, S. Libs, A. Kiennemann, A. Barama, Catal. Today, 113 (2006), pp. 194–200
40 N. Sahli, C. Petit, A.C. Roger, A. Kiennemann, S. Libs, M.M. Bettahar, Catal. Today, 113 (2006), pp. 187–193
41 G. Valderrama, M.R. Goldwasser, C.U. de Navarro, J.M. Tatibouet, J. Barrault, C. Batiot-Dupeyrat, F. Martınez, Catal. Today, 107–108 (2005), pp. 785–792
42 S.M. de Lima, Ć.M.A. Pena, Ć.J.L.G. Fierro, Ć.J.M. Assaf, Catal. Lett., 124 (2008), pp. 195–203
43 F. Besenbacher, I. Chorkendorff, B. S. Clausen, B. Hammer, A. M. Molenbroek, J. K. Norskov, I. Stensgaard, Science 279 (1998) 1913-1915
44 Y.-H. Chin, D.L. King, H.-S. Roh, Y. Wang, S.M. Heald, J. Catal., 244 (2006), pp. 153–162
45 H.S. Bengaard, J.K. Nørskov, J. Sehested, B.S. Clausen, L.P. Nielsen, A.M. Molenbroek, J.R. Rostrup-Nielsen, J. Catal., 209 (2002), pp. 365–384
46 J. R. Rostrup-Nielsen, I. Alstrup, Catal. Today 53 (1999) 311-316
47 M: Rodríguez-Rodríguez, J. L. Phase Transitions, 2 (1982) 241-246
48 C.-C. Kim, C. Wang, Y.-C. Yang, Y.-K. Hwu, S.-K. Seol, Y.-B. Kwon, C.-H. Chen, H.-W. Liou, H.-M. Lin, G. Margaritondo, J.-H. Je, Mat. Chem. Phys. 100 (2006) 292-295
49 A. Venugopal, J. Aluha, M. S. Scurrell, Cat. Lett. 90 (2003) 1-6
50 T. Yang, L. Zhang, X. Li, D. Xia, J. Alloys and Comp. 492 (2010) 83-87
51 C.D. Wagner, A.V. Naumkin, A. Kraut-Vass, J.W. Allison, C.J. Powell, J.R. Rumble Jr., NIST X-ray Photoelectron Spectroscopy Database, Version 3.4, National Institute of Standards and Technology, Gaithersburg, MD, 2003, http://srdata.nist.gov/xps/
52 I. Czekaj, F. Loviat, F. Raimondi, J. Wambach, S. Biollaz, A. Wokaun, Appl. Catal. A, 329 (2007), pp. 68–78
53 W. Fan, X. G. Gong, Surf. Sci. 562 (2004) 219-225
54 P. M. Holmblad, J. Hvolbaek Larsen, I. Chorkendorff, J. Chem. Phys. 104 (1996) 7289-7295
55 W. K. Józwiak, M. Nowosielska, J. Rynkowski, Appl. Catal. A: Gen. 280 (2005) 233-244